water

MDPI

Article

Sodium Alginate-Based Composite Films for Effective Removal of Congo Red and Coralene Dark Red 2B Dyes: Kinetic, Isotherm and Thermodynamic Analysis

Amina Mokeddem [1], Samir Benykhlef [1,2], Amine Ahmed Bendaoudi [1], Nacer Boudouaia [1], Hacene Mahmoudi [3], Zohra Bengharez [1,*], Seda Demirel Topel [4] and Önder Topel [5]

[1] Laboratory of Advanced Materials and Physicochemistry for Environment and Health, Djillali Liabes University, Sidi Bel Abbes 22000, Algeria
[2] Ecole Supérieure en Sciences Appliquées de Tlemcen, ESSA-Tlemcen, BP 165 RP Bel Horizon, Tlemcen 13000, Algeria
[3] Faculty of Technology, University Hassiba Benbouali of Chlef, Chelf 02000, Algeria
[4] Department of Electrical and Electronics Engineering, Faculty of Engineeringand Natural Sciences, Antalya Bilim University, Dosemealtı, Antalya 07190, Turkey
[5] Department of Chemistry, Faculty of Science, Akdeniz University, Antalya 07058, Turkey
* Correspondence: dzbengharez@yahoo.fr; Tel.: +213-5-41-76-15-78

Abstract: The present study aimed to investigate the adsorption capacity of two anionic dyes, namely, Congored (CR) and Coralene Dark Red2B (DR), onto prepared alginate (Alg) and chitosan(Cs) biopolymer films. The two biopolymers were combined at different mass ratios using a "solvent-cast" process to incorporate their unique properties and evaluate their effectiveness in removing the dyes. All samples were characterized by means of Fourier transform infrared spectroscopy (FTIR), differential scanning calorimetry (DSC), scanning electron microscopy (SEM) and determination of point of zero charge (pH_{pzc}). The swelling ratios were determined by gravimetric measurements. The effects of pH, adsorption time, thickness, temperature and initial concentration of CR and DR dyes on the adsorption results were studied systematically. The dye adsorption kinetics showed that the Alg/Cs films at % proportions of 75/25, 50/50, 25/75 and 0/100 reached equilibrium from 30 min to 180 min with high removal efficiencies that varied between 222.30 mg/g and 842.36 mg/g. The adsorption mechanism of CR and DR onto the synthesized biofilms was confirmed through Langmuir isotherm and the kinetics fitted well by the pseudo-second-order model, suggesting a monolayer and chemisorption process. The thermodynamic results demonstrated the spontaneity and the feasibility of the process as well as the exothermic nature. Hence, the findings revealed that the Alg/Cs biofilms could be employed as potential natural adsorbents for the removal of anionic dye pollutants from aqueous environments.

Keywords: alginate; chitosan; film; anionic dye; adsorption; performance

Citation: Mokeddem, A.; Benykhlef, S.; Bendaoudi, A.A.; Boudouaia, N.; Mahmoudi, H.; Bengharez, Z.; Topel, S.D.; Topel, Ö. Sodium Alginate-Based Composite Films for Effective Removal of Congo Red and Coralene Dark Red 2B Dyes: Kinetic, Isotherm and Thermodynamic Analysis. *Water* **2023**, *15*, 1709. https://doi.org/10.3390/w15091709

Academic Editor: Jesus Gonzalez-Lopez

Received: 28 February 2023
Revised: 22 April 2023
Accepted: 24 April 2023
Published: 27 April 2023

1. Introduction

The textile industry is recognized as one of the most polluting industries worldwide that consumes large amounts of chemical products, thus generating considerable quantities of liquid and solid waste endangering both human health and the natural environment [1]. Dyes are among the contaminants frequently found in textile industry wastewaters. According to recent statistics [2], the global market of textile dyes rose annuallyat a growth rate of8.13% over the period of 2016–2023. The presence of dye pollutants in the wastewater, even at low concentrations, can bring adverse impacts on both human beings and aquatic organisms. Indeed, aquatic life suffers important damages due to a net reduction in the level of dissolved oxygen and the rate of photosynthesis caused by the presence of dyes in water bodies, which prevent sunlight from penetrating water [3]. Furthermore, human exposure to dyes via inhalation, digestion or skin exposure can cause serious health issues,

including dermatological diseases, nervous system disorders, bladder cancer, colon cancer and colorectal cancer [3,4]. Numerous research has reported the toxicity, mutagenicity and the carcinogenic potentiality of textile dyes [4,5]. Among these dyes, azo dyes are the most used synthetic dyes worldwide in the dyeing processes, cosmetics, food, paper printing, tanning, pharmaceutical industry, etc. However, the textile industry represents 80% of these applications [3]. Due to their complex aromatic ring structures, azo dyes are recognized as the most toxic textile dyes [3,5]. Faced with this complex problem, several governments have strengthened their legislation regarding the management of dye-rich wastewaters and treatment technologies to ensure a safe and clean environment for the next generations [3].

Several physical, chemical and biological methods, including membrane technology, photocatalytic degradation, coagulation/flocculation, electrocoagulation, aerobic and anaerobic microbial degradation, adsorption and chemical oxidation, have been used to treat dye effluents to eliminate the hazardous dyes from wastewater [3,5,6]. Particularly, adsorption, being a surface phenomenon, due to its efficiency, low treatment cost, simplicity and recycling facilities, is considered to be the most effective method for the removal of dyes where the type of adsorbent plays a crucial role in the process [6,7]. In this sense, numerous raw and modified materials were successfully used to treat dye-contaminated water, comprising activated carbon, zeolites, metal oxides, silica gel, bioadsorbents and polymer-based materials [3,8–12]. The use of biopolymer-based materials as advanced adsorbents for the removal of dyes has attracted great interest in recent years [12,13].

In this context, the development of films composed of natural biopolymers, such as alginate(Alg) and chitosan(Cs), used to be an eco-friendly alternative for the adsorption of dyes and remediation of contaminated water sources [14]. Alginate as a valuable natural polymer is composed of two monomers, namely, (1 → 4) β-D-mannuronate and (1 → 4) β-L-guluronate, and it also contains hydroxyl and carboxyl groups in the molecule [15]. Alginate is known for its high water solubility, safety and ionic gelation capacity in the presence of cations like Ca^{2+} [16].

Chitosan is a linear polysaccharide obtained from the deacetylation of chitin, a major component of crustacean shells, which contains (1–4) linked D-glucosamine and N-acetyl-D-glucosamine monomers. Despite the interesting properties of chitosan, making it one of the most economical biopolymers to remove dyes, it is often modified to composite material for effective adsorption of a large variety of these pollutants [14,17]. Indeed, the use of alginate and chitosan as a single adsorbent may have limited properties, which may interact with only cationic or anionic dyes, limiting the utilization in the complex wastewater treatment [18]. That is why both biopolymers in a form of composite film could interact with various ions to make stable materials via electrostatic attractions, as well as complexation [14]. Due to the anionic and cationic nature of alginate and chitosan, respectively, alginate-chitosan gels can be easily obtained through electrostatic interactions between the carboxylate moieties on alginate -COO^- and the protonated amines on chitosan -NH_3^+. This combination leads to the formation of material with improved physicochemical properties in terms of structural strength and mechanical stability.

Accordingly, the present study aims to shed light on the adsorption of two main hazardous dyes, Congo red (CR) and Coralene Dark Red2B (DR), onto the biofilms based on alginate and protonated chitosan. These two dyes are benzidine-based anionic diazo dyes and are known to break down into benzidine, a high carcinogenic agent and mutagen for humans [5]. Extensive research has been conducted on the removal of CR by various materials; however, there is a clear gap for DR in the recent scientific literature. Only one paper reported the photocatalytic degradation of Coralene red dye by titanium dioxide nanoparticles (TiO_2NPs) [19].

The main goals of this paper are: (i) to develop composite films based on natural alginate and chitosan via facile method, (ii) to characterize these films by using various analytical techniques and (iii) to investigate their effectiveness in removing CR and DR dyes under diverse experimental conditions. To our knowledge, this is the first time that Coralene Dark Red 2B adsorption on composite film was investigated and compared.

2. Materials and Methods

2.1. Materials

Sodium alginate of number- and mass-average molar mass (Mn and Mw) of about 195,000 and 350,000 g mol^{-1}, respectively, polymolecular index (Ip) 1.8 and with a ratio of mannuronate residues to guluronate residues (M/G ratio) of 0.5 was purchased from Degussa Company (Essen, Germany). Chitosan (Mn) 40,000 was supplied by Sigma-Aldrich (St-Quentin-Fallavier, France) in powder form (commercial high molecular weight chitosan REF/419419). Other reagents were of analytical grade. Congo red RC($C_{32}H_{22}N_6Na_2O_6S_2$, Mw = 696.66 g/mol), a textile dye, was supplied by Sigma Aldrich company (St-Quentin-Fallavier, France). Coralene Dark Red2B ($C_{23}H_{26}ClN_5O_7$, Mw= 519.93 g/mol), a textile dye, was manufactured by the CHT group (Montlingen, Switzerland) and delivered by the unit of production of the blue jean and the cotton gabardine Denitex (Sebdou, Algeria).

2.2. Preparation of Alg and Cs Film Solutions and Formation of Alg/Cs Films

2.2.1. Preparation of Alg Film

A sodium alginate film was prepared by casting/solvent evaporation according to the following procedure: A 1% (*w/w*) sodium alginate solution was prepared by dissolving 1 g of powdered sodium alginate in 100 mL of distilled water (pH = 6.5) with continuous stirring for about 2 h at room temperature using a magnetic stirrer. The resultant solution was filtered using a vacuum filtration system in order to remove residual contaminants. The solution was then poured into Petri dishes and dried at 30 °C for 24 to 48 h. Once the Alg film was completely dry, it was removed from the Petri dishes and stored in a desiccator.

2.2.2. Preparation of Cs Film

The chitosan film was prepared with the same procedure above, but utilizing an acetic acid aqueous solution 0.17 M. The formed chitosan-H^+ film was detached from the Petri dishesand immersed in NaOH solution 0.1 M several times until the Cs film was neutralized. The chitosan film was then dried again at 30 °C for 72 h.

2.2.3. Preparation of the Alg/Cs Films

The prepared Alg and Cs solutions were mixed dropwise under continuous magnetic stirring for 5 h at room temperature and at different Alg/Cs ratios to obtain uniformly dispersed solutions. The electrostatic interaction between Alg and Cs molecules is represented in Figure 1.

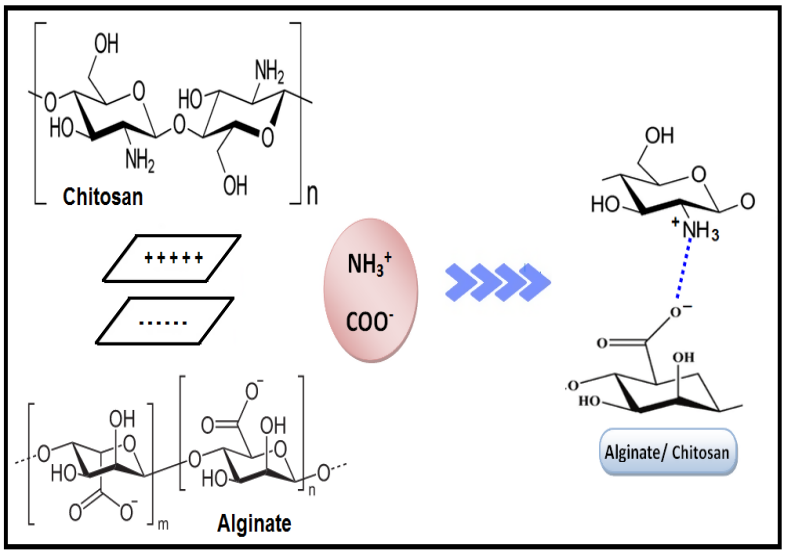

Figure 1. Schematic representation of the ionic cross-linking of Alg and Cs.

The mixed Alg/Cs solutions were then poured into Petri dishes and dried at 30 °C for 72 h. The formed composite films were then removed from the Petri dishes and immersed in 0.1 M of NaOH for 1 h until they were neutralized. Five Alg/Cs films were fabricated and labeled as M1, M2, M3, M4 and M5, respectively. These designations corresponded to the Alg/Cs ratios of 100/0, 75/25, 50/50, 25/75 and 0/100, respectively. The thickness of each film was measured at five distinct points on the surface, utilizing a digital micrometer (Tesamaster, Swiss) to the nearest 0.001 mm. The mean values of the measurements were subsequently calculated [20].

2.3. Characterization Techniques

2.3.1. Fourier-Transform Infrared Spectrometry (FTIR)

The FTIR spectra of the Alg/Cs films were recorded on a Bruker ATR spectrometer in the range 400–4000 cm^{-1}.

2.3.2. Scanning Electron Microscopy (SEM)

The surface and cross-sectional morphologies of the samples were investigated using a scanning electron microscope (SEM) (ZEİSS LEO 1430, Carl Zeiss, Oberkochen, Germany).

2.3.3. Differential Scanning Calorimetry (DSC)/Thermal Gravimetric Analysis (TGA)

DSC thermograms were obtained using a differential scanning calorimeter (Netzsch DSC-214 polyma, Selb, Germany). A total of 10 mg of the sample was put in the crucible and heated from 25 to 500 °C at a heating rate of 10 °C/min under a nitrogen atmosphere. TGA analysis was performed using a thermogravimetric analyzer (Discovery SDT 650) at a heating rate of 10 °C/min to 1000 °C.

2.3.4. Surface Zeta Potential

Zeta potential measurements were conducted with a zeta potential analyzer (Nano ZS, Malvern, UK) in the pH range of 2–12.

2.3.5. Point of Zero Charge pH_{pzc}

The pH_{pzc} is a key parameter in the adsorption process since it permits us to better understand the surface adsorption mechanism. It corresponds to the pH at which the adsorbent surface has a net charge of zero. The pH_{pzc} of the prepared films was evaluated according to the experimental protocol described in a previous paper [21]. For this, 1 cm^2 of the prepared film was shaken for 24 h with 50 mL of 0.01 M NaCl solution at different initial pH values ranging from 2–12, and the final pH was measured. The pH_{pzc} corresponds to the point where the curve of pHfinal–pHinitial versus pHinitial crosses the abscise axis. The initial pH was adjusted by using 0.1 M HCl or NaOH solutions.

2.4. Swelling Study

A completely dried film (1 cm^2 surface) was weighed and immersed in the desired solution at room temperature. At regular time intervals, the film was filtered, excess water was removed and weighed to constant weight. The percent swelling was calculated from the following equation:

$$S\% = [(m_t - m_0)/m_0] \times 100 \quad (1)$$

where $S\%$, m_t and m_0 are the percent swelling, weight of swollen films and weight of dry films, respectively.

2.5. Preparation and Analysis of the CR and DR Dyes

As textile anionic dyes, CR and DR were selected for the adsorption tests (Figure 2). A stock solution of CR and DR dyes at a concentration of 1 $g{\cdot}L^{-1}$ were prepared in double distilled water. All working solutions at desired concentrations were obtained by successive dilutions. The dye concentrations were measured using a double-beam UV–Vis spectrophotometer (SPECORD 210 Plus Analytik Jena, Jena, Germany) at the

maximum wavelength λ_{max} = 498 and 500 nm for CR and DR, respectively, and via standard calibration curve.

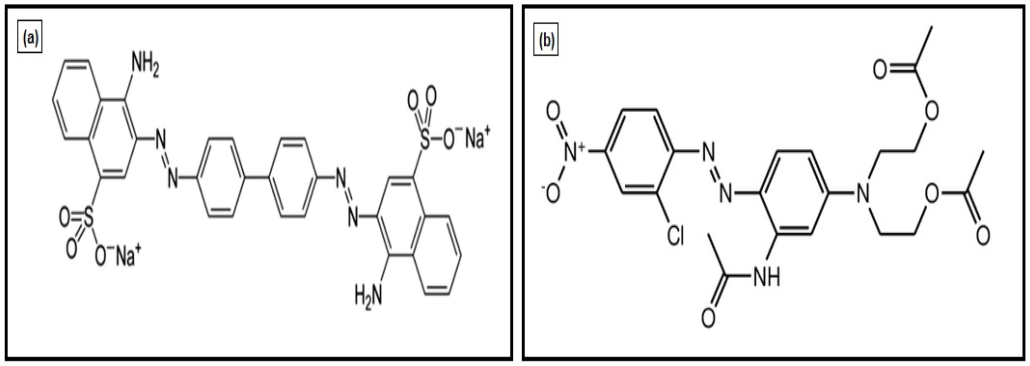

Figure 2. Chemical structure of (**a**) Congo red (CR); (**b**) Coralene Dark Red2B (DR).

2.6. Adsorption Experiments

The adsorption performance of Alg/Cs films towards CR and DR dyes was investigated in a batch system under various experimental conditions including contact time (1–300 min), initial dye concentration (50–300 mg.L^{-1}), pH of the solution (4–10), temperature (10–40 °C) and thickness of the film (M2: 0.12, 0.29, 0.32 and 0.35 mm; M3: 0.24, 0.30, 0.36 and 0.41 mm; M4: 0.29, 0.38, 0.39 and 0.45 mm; M5: 0.31, 0.38, 0.42 and 0.49 mm). Briefly,1 cm^2 of Alg/Cs film was immersed into 50 mL of dye solutions at pre-set pH conditions, dye concentration, film thickness and temperature under a constant agitation speed of 500 rpm for definite time intervals. After the adsorption test, the suspension was filtered with a 0.45 µm pore size filter and the remaining dye concentration was analyzed with the UV–visible spectrophotometer (SPECORD 210 Plus Analytik Jena, Germany) at λ_{max} of each dye. All the tests for CR and DR removal were performed in triplicate.

The equilibrium adsorption capacity q_e (mg/g) and adsorption efficiency AE (%) were estimated by using the following equations:

$$q_e = (c_0 - c_e) \times \frac{v}{m} \quad (2)$$

$$AE(\%) = \frac{c_0 - c_e}{c_0} \times 100 \quad (3)$$

where C_0, C_e, m, V and q_e are the initial dye concentration (mg/L), dye concentration at equilibrium (mg/L),the adsorbent mass (g), volume (L) of the dye solution, respectively.

2.7. Different Models and Equations Used in Data Analysis

The mathematical equations related to the different kinetic and isotherm models applied for assessing the adsorption performance of Alg/Cs films towards CR and DR dyes, as well as equations for the determination of thermodynamic parameters, are summarized in Table 1.

Table 1. Models and equations used in data analysis.

Models	Type of the Model	Equations	
Kinetic models	Pseudo-first-order	$\log(q_{eexp} - q_t) = \log_{qecal} - k_1 \times t$	[22]
	Pseudo-second-order	$t/q_t = 1/k_2 {q_{ecal}}^2 + t/{q_{ecal}}^2$	[22]
Isotherm models	Langmuir	$c_e/q_e = 1/K_L q_m + c_e/q_m$	[22]

Table 1. *Cont.*

Models	Type of the Model	Equations	
	Freundlish	$\log q_e = 1/n \log c_e + \log K_F$	[22]
Thermodynamic study	Van't Hoff equation	$\ln K^\circ = \Delta S^\circ/R - \Delta H^\circ/RT$ $\Delta G^\circ = -RT \ln K^\circ$ $K^\circ = \frac{q_e}{C_e}$	[13]

Note(s): q_e and q_t (mg·g^{-1}): the adsorbed amounts at equilibrium and at time t; k_1 (min^{-1}) and k_2 (g·mg^{-1}·min^{-1}): the rate constants of pseudo-first-order and pseudo-second-order models; C_e (mg·L^{-1}): equilibrium concentration of the adsorbate; q_m (mg·g^{-1}): the maximum adsorption capacity; K_L (L·mg^{-1}): the Langmuir adsorption constant; K_F (mg·g^{-1}) (L·mg^{-1})$^{1/n}$ and n: the Freundlich isotherm constants; K°: the thermodynamic equilibrium constant; ΔG° (kJ/mol): standard free energy change; ΔH° (kJ·mol^{-1}) and ΔS° (J·K^{-1}mol^{-1}): change in enthalpy and entropy; T (K): the absolute temperature; R: universal gaz constant (8.314 J·mol^{-1}·K^{-1}).

3. Results and Discussion

3.1. Characterization of Alg/Cs Biofilms

3.1.1. FTIR Spectra

The FTIR spectra of the samples, namely, M1, M2, M3, M4 and M5, are represented in Figure 3. The figure revealed that all the biofilms have hydroxyl (-OH) functional groups due to the broad O-H stretching vibrations at 3300 cm^{-1}. The C-H stretching of CH_2 groups in the biofilms is assigned to the peaks located at 2926–2906 cm^{-1} and 2873–2865 cm^{-1}.

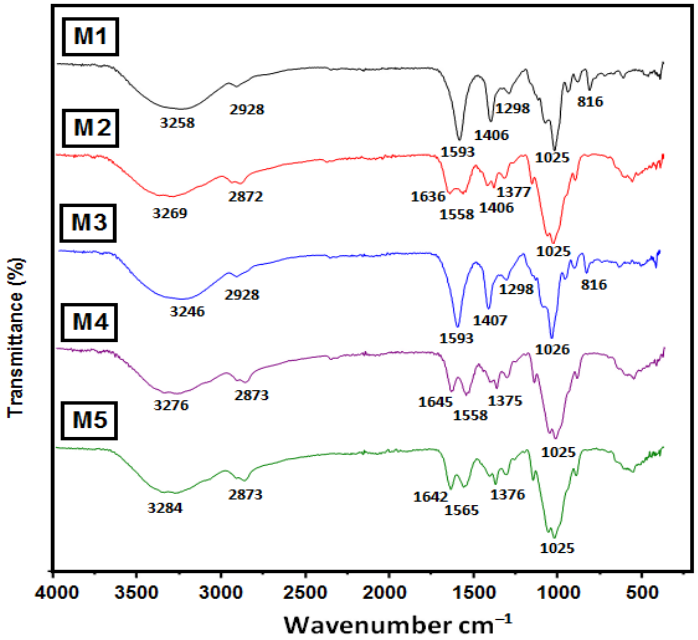

Figure 3. FTIR spectra of Alg/Cs films prepared at different ratios.

The M1 composite film solely comprises alginate molecules that possess carboxylate and hydroxyl functional groups. The absorption peaks at 1647 and 1410 cm^{-1} are ascribed to the asymmetric and symmetric stretching vibrations of the carbonyl group (C=O) in the carboxylate group, respectively [23]. Furthermore, the band at 1027 cm^{-1} corresponds to the C-O-C stretching vibration, signifying the saccharide structure of alginate [23]. In the case of the composite films M2, M3 and M4, containing 25%, 50% and 75% chitosan, respectively, the amine vibrations are expected due to the existence of amine functional groups in the chitosan molecule. The stretching peak of amine (NH_2) most likely exists under the broad band of the hydroxyl group at 3300 cm^{-1}. The absorption band of the carbonyl (C=O) stretching of the primer amine and the bending vibrations of -NH are evident at 1641–1634 cm^{-1} and 1377 cm^{-1} [24].

The IR spectra of the M1, M2 and M3 films demonstrate less intense bands for both the -COO^- group from alginate and the NH_3^+ group of protonated chitosan, indicating successful interactions between the positive charges of -NH_3^+ and the negative charges of -COO^-. Moreover, the IR spectrum of the M5 film illustrates two bands at 1646 cm^{-1} and 1548 cm^{-1}, corresponding to NH_2 and N-H groups of chitosan which do not appear in the alginate spectrum [24].

3.1.2. SEM Analysis of the Alg/Cs Biofilms

According to the SEM images, all M1–M5 films exhibit a smooth surface morphology, as depicted in Figure 4 (top view). The M1 and M5 films, which contain 100% alginate and 100% chitosan, respectively, also display a smooth cross-section morphology. Conversely, M2, M3 and M4 display a layered structure in the cross-section of the corresponding films, owing to the mixed combination of alginate and chitosan, as represented in Figure 4. This observation provides additional evidence of the successful integration of alginate and chitosan polymers into a single film structure.

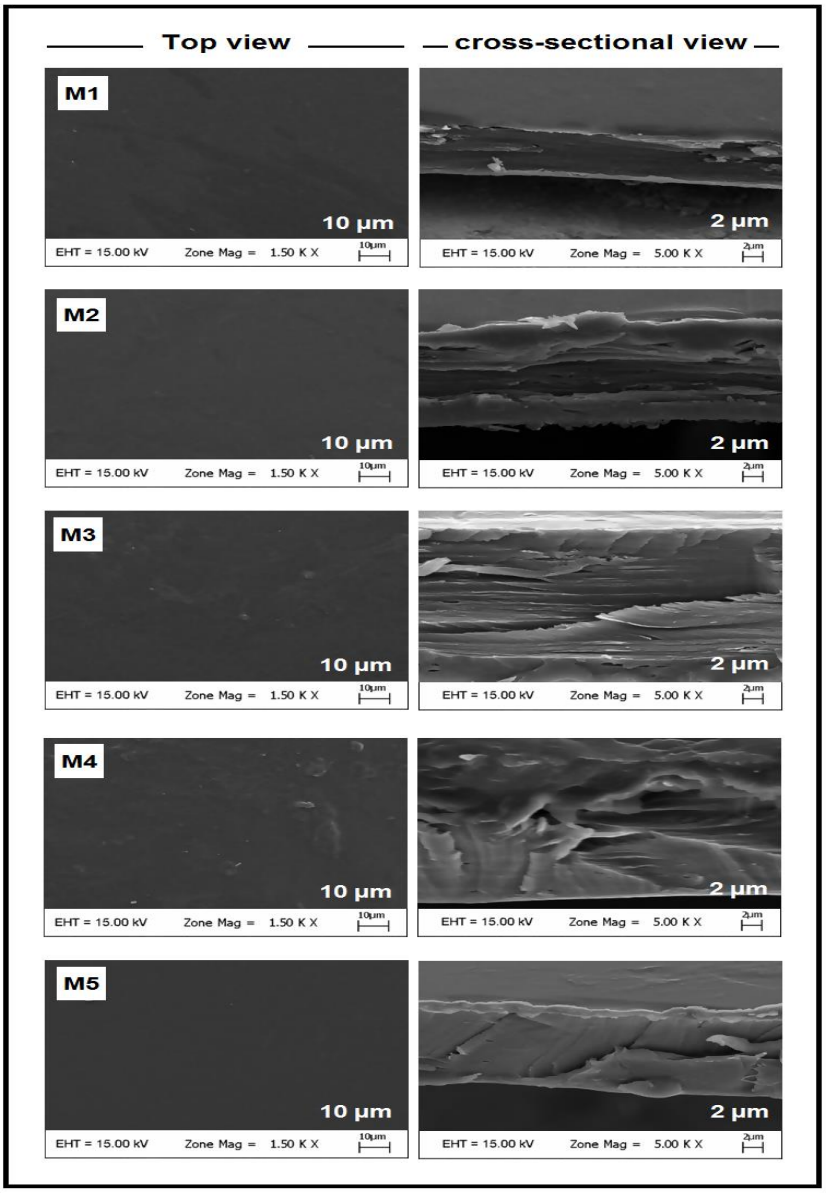

Figure 4. SEM images of Alg/Cs films.

3.1.3. DSC (Differential Scanning Calorimetry)/ATG (Thermal Gravimetric Analysis)

DSC is a crucial tool for investigating the thermal behavior of polymers. As demonstrated in Figure 5, the DSC curves exhibit endothermic peaks at 88.6, 78.4, 83.9, 72.3 and 66.9 °C for M1, M2, M3, M4 and M5 biofilms, respectively. These peaks are attributed to the evaporation of residual water associated with the hydrophilic groups present in the polymer structure (Figure 5). In addition, exothermic peaks appear between 235–295 °C in a range intermediate to the degradation temperatures of pure alginate observed at 233.3 and 284.4 and chitosan at 301.6 °C. This finding confirms the interaction between alginate and chitosan, while small peaks in both M2 and M3 biofilms suggest the non-association of a fraction of alginate with chitosan [25,26].

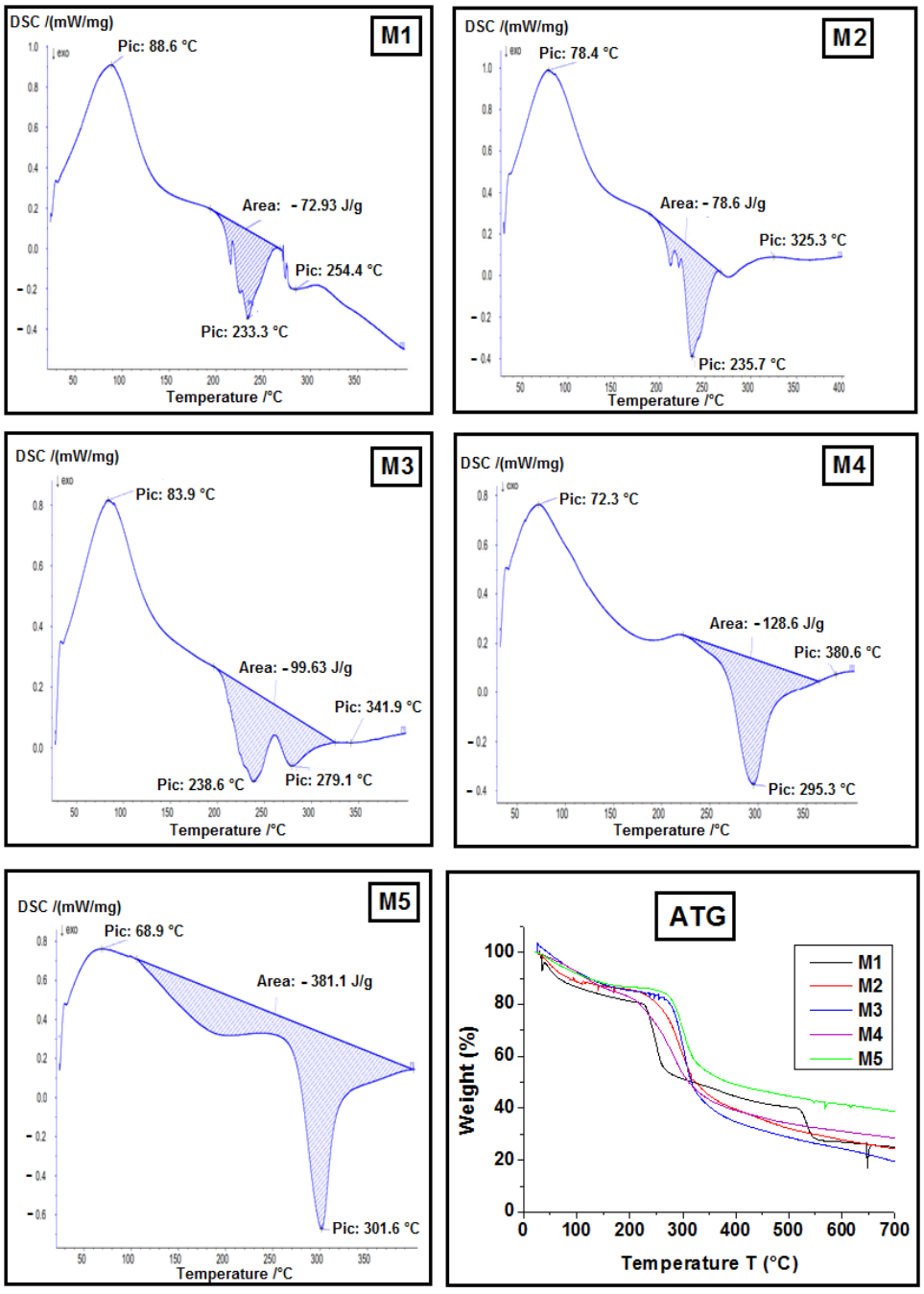

Figure 5. DSC and ATG analysis of Alg/Cs films.

According to DSC thermograms, the enthalpy values were found to be 72.93, 78.46, 99.63, 126.8 and 381.1 J/g for M1, M2, M3, M4 and M5, respectively. This increase can be explained by the increase in crystallinity of the polymer related to the rigid crystalline nature and presence of strong inter/intra molecular hydrogen bond in the structure of the biofilm matrix. In addition, the results of the TGA showed two main thermal decomposition stages (Figure 5). For all films, the first weight loss of approximately 10% occurred between 30 and 150 °C during the first stage related to the evaporation of water moieties on the surface [27]. Then, the second weight loss phase was observed for all films between 150 and 385 °C. This stage is considered as the largest weight loss (around 50%),which could be explained by the thermal degradation of film-forming components of pure Alg, Cs and composite films. The main degradation peaks of M2, M3 and M4 occurred in a range intermediate to the degradation temperatures of pure alginate and chitosan films, confirming the interaction between alginate and chitosan in accord with results from DSC analysis.

3.2. Swelling Behavior of Alg/Cs Biofilms

The swelling behavior of Alg/Cs films at different pH values and as a function of time is presented in Figure 6. It is evident from Figure 6a that the degree of swelling of Alg/Cs films varies significantly. The results reveal that the swelling rate is directly proportional to the weight ratio of chitosan in the composite films. The initial 20 min of the swelling process shows a rapid increase in swelling, followed by a gradual decrease until the equilibrium is reached at 60 min. This trend is observed for all the composite films. Notably, the non-crosslinked chitosan film M5 has a higher swelling rate of 375% compared to that of crosslinked film, which is in accordance with literature reporting that the introduction of the crosslinking agent into the hydrogel matrix leads to a decrease in its swelling capacity [28].

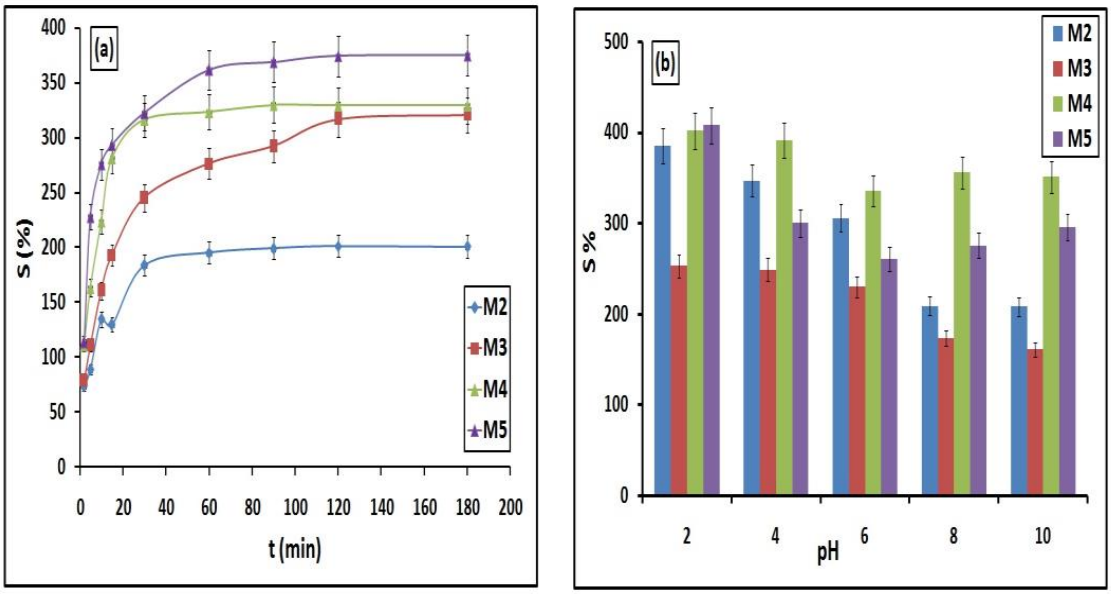

Figure 6. Swelling behavior of Alg/Cs films: (**a**) effect of contact time, (**b**) effect of pH.

On the other hand, Figure 6b displays the degree of swelling S% of the synthesized films at various pH. As can be observed, all films show a decrease in swelling capacity with an increasing pH. Indeed, at acid pH values, the carboxylic groups of the alginate, as well as the amines of chitosan, are protonated, contributing to the increase in electrostatic repulsion forces between the charged sites, thereby producing more space to absorb water molecules. However, when pH increases, the electrostatic interactions between $-NH_3^+$ and $-COO^-$ become stronger, which should decrease the swelling ration of the film [29,30].

3.3. Adsorption Tests

3.3.1. Effect of Contact Time

In terms of adsorption analyses, saturation time plays a pivotal role. Figure 7 depicts the impact of contact time on the removal of CR and DR by the prepared films. As can be seen, the adsorbed amount of each dye increased rapidly during the first 10 min and then slowed down until reaching equilibrium state, where the adsorption capacity remains constant. Maximum CR adsorption capacities of 336.07, 627.49, 842.36 and 745.64 mg/g are obtained for M2, M3, M4 and M5, respectively, while the films showed slower capacities toward DR dye ranging from a minimum of 222.30 to a maximum of 315.52 mg/g. The better adsorption of CR compared to DR could be related to the chemical structure of the dye.

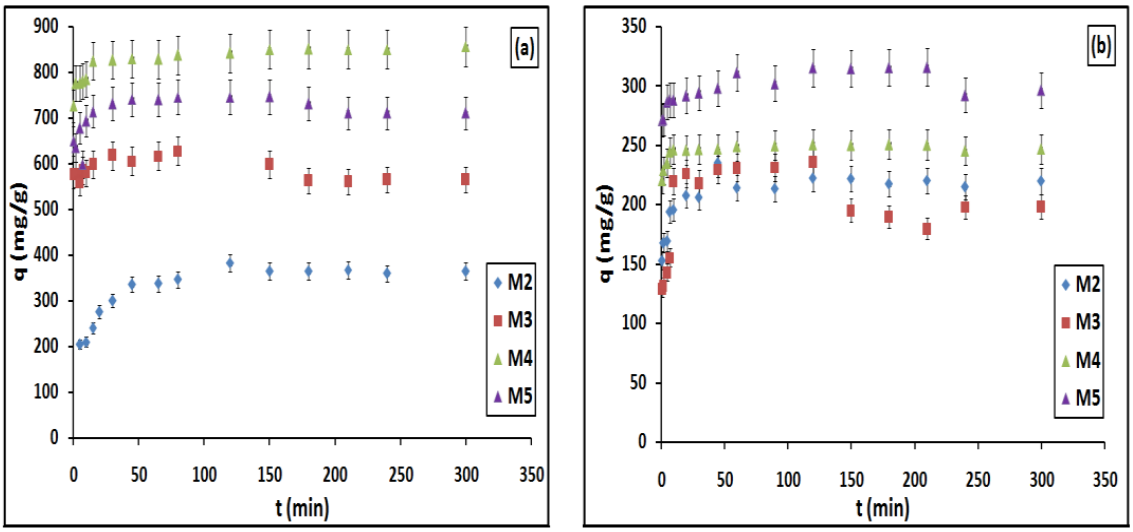

Figure 7. Effect of contact time on the adsorption of (**a**) CR, (**b**) DR onto Alg/Cs film.

The initial phase of the adsorption experiment showed a rapid increase in the adsorption capacity, attributed to the availability of numerous vacant sites on the adsorbent surface. However, as the contact time increased, the number of vacant sites decreased, resulting in a reduced adsorption capacity. In addition, with the increasing content of chitosan into the composite films, the adsorption capacities increased significantly due to the provision of more adsorption sites by chitosan and to the charge neutralization. This result is in accordance with those indicated by Zhao et al. (2020) [18] when examining the removal of anionic Acid Black-172 dye onto composite foams based on chitosan and sodium alginate. They found that the adsorption capacity was strongly dependent on the mass ratio of chitosan to sodium alginate.

3.3.2. Effect of pH

Initial pH is a critical parameter affecting the adsorption process, and therefore, it was studied in the range of 4 to 10 at room temperature, while the initial concentrations of CR and DR and the contact time were fixed at 200 mg·L^{-1} and 50 min, respectively. The results are presented in Figure 8a.

Firstly, in acidic medium (pH = 4), M4 film (the Alg/Cs ratio: 25/75) showed thehighest adsorption capacity for CR (735.5 mg/g) compared to other films and to that of DR dye (510.3 mg/g). These results validate the exceptional adsorption ability and efficiency of the M4 film towards CR dye, especially under acidic conditions. Moreover, based on the value of pH_{pzc} of M4 (5.9, Figure S1), the adsorbent surface acquires a positive charge at a pH below 5.9 and thus promotes the removal of the negatively charged dye (CR and DR). Additionally, a maximum adsorption capacity of M5 film was observed at low pH, which can be explained by the zeta potential values (Table S1) where the film exhibits the largest

positive charge (78.63 ± 2.15 mV) at pH = 4, thereby enhancing the adsorption efficiency of both anionic dyes. This outcome reflected the strong electrostatic interaction formed at low pH between the protonated surface of both films and dyes negatively charged. A similar behavior was observed by ALSamman and Sánchez [31] for the adsorption of Methyl orange anionic dye onto chitosan- and alginate-based hydrogels, where a maximum removal efficiency was found at pH = 3.0. However, an increase in pH values led to a decrease in the adsorbed numbers of dyes due to the excess of OH^- ions, which deprotonate the positive sites on the composite film, impairing the adsorption process.

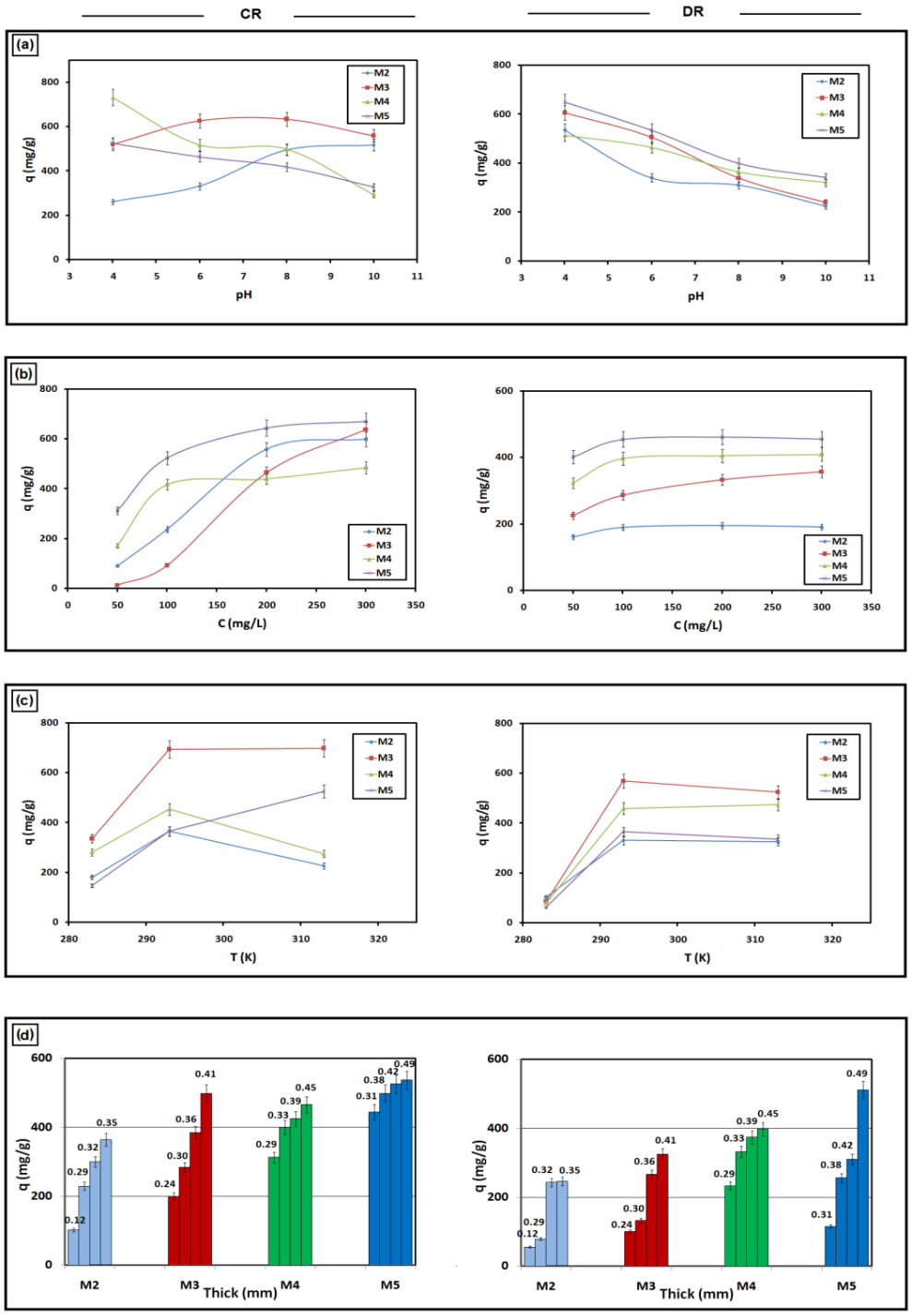

Figure 8. Effect of (**a**) pH, (**b**) initial concentration, (**c**) temperature and (**d**) film thickness on the adsorption of CR and DR dyes onto Alg/Cs films.

The lower adsorption performance of M2 film observed at low pH, especially for RC dye, could be explained by the largest number of negative charges on its surface confirmed by the value of zeta potential −71.9 ± 4.86 mV (Table S1) achieved at pH 4, leading to electrostatic repulsions with the anionic dyes and thus, to a decrease in the adsorption capacity. Recent works [32] on dye adsorption onto alginate/lignin composite hydrogel beads revealed similar behavior where the highest adsorption capacity of 240 mg/g was attained at pH = 12. Moreover, the optimum adsorption capacity of CR onto M3 film was obtained at pH = 6–8, which is in line with the pH_{pzc} estimated at 8.3, making the adsorption efficiency less favorable above this value. This is in accordance with findings of Inas et al. [33] who reported an optimal pH of 6.5~7 for CR adsorption onto limestone–chitosan–alginate nanocomposite.

3.3.3. Effect of Initial Concentration

The adsorbed dye amount is one of the important driving forces that affects the adsorption [34]. Figure 8b illustrates the effect of initial CR and DR dye concentrations from 50 mg to 300 mg. This result indicates that by increasing the initial dye concentration, the adsorption capacity increased, which could be explained by the presence of a high number of CR and DR molecules, making more contact between dye and adsorbent [35,36]. However, the effect of initial DR concentration on the adsorption efficiency appears not significant compared with CR, confirming the less adsorption affinity of DR onto the Alg/Cs biofilms, probably due to its chemical structure and molecular rearrangement [37]. The maximum amount of adsorption of each dye was achieved at an initial dye concentration of 300 mg/L.

3.3.4. Effect of Thickness

The impact of film thickness was investigated under the experimental conditions cited in Section 2.6 while keeping the other parameters constant. The results, presented in Figure 8d, clearly indicate that the adsorption potential of the films for both dyes is affected by variations in the film thickness. Notably, the increase in thickness led to a significant enhancement in dye adsorption capacity. M5 film with a thickness of 0.49 mm exhibited high CR and DR adsorption capacities of 536.28 and 510.16 mg/g, respectively. The enhanced adsorption performance observed with increasing film thickness can be attributed to the expansion of the diffusion path, which results in greater swelling of the film and thus facilitates dye uptake [38].

In addition, it is known that the available surface area is directly proportional to the film thickness, which can explain the higher adsorption capacities observed with increasing thicknesses.

3.3.5. Adsorption Isotherms and Kinetic Studies

The kinetic analysis provides crucial details on the CR and DR adsorption mechanisms onto the Alg-Cs films. Pseudo-first-order and pseudo-second-order models were applied for modelling the experimental data. Optimum conditions (pH: 4 except for CR adsorption by M2 (pH: 10), initial dye concentration: 300 mg·L^{-1},room temperature, Time: 45–50 min) lead to the determination of parameters associated to the kinetics models. The adsorption capacities (q_{cal}, q_{exp}), regression coefficients (R^2) and constant rates (k_1 and k_2) are depicted in Table 2. The adsorption of CR and DR dyes showed excellent fitting with pseudo-second-order, with high values of R^2 near to 1. In addition, the theoretical q_e (cal) values were in accordance with the results calculated from the experimental data. This suggests chemisorption involving various interactions between dyes and Alg/Cs functional groups. A higher correlation for the pseudo-second-order model has also been shown for CR removal by using various and similar adsorbents [39,40]. Additionally, the pseudo-first-order kinetic model gave lower R^2 and the experimental and theorical adsorption capacities were not in agreement, attesting that this model is not appropriate to describe the adsorption of both dyes onto the Alg/Cs films.

Table 2. Pseudo-first-order and pseudo-second-order model parameters/Langmuir and Freundlich isotherm parameters for the adsorption of CR and DR onto the Alg/Cs biofilms.

		CR				DR			
	Biofilms	**M2**	**M3**	**M4**	**M5**	**M2**	**M3**	**M4**	**M5**
Pseudo-first-order	q_e (exp) (mg/g)	494.27	627.49	842.36	745.74	222.30	236.18	249.78	315.52
	q_e (cal)	536.86	489.29	500.16	546.39	453.95	462.10	290.58	424.05
	k_1 (min^{-1})	0.15	0.04	0.03	0.05	0.032	0.035	0.036	0.025
	R^2	0.968	0.812	0.909	0.933	0.944	0.815	0.702	0.751
Pseudo-second-order	q_e (cal)	500	625	833.33	769.23	222.22	238.09	250	312.5
	k_2 (g/mg·min) (10^{-4})	5.1	3.1	2.3	17	50.5	20.6	160.2	26.4
	R^2	0.999	0.997	0.999	0.998	0.999	0.999	0.999	0.999
Langmuir isotherm	q_m (mg/g)	357.14	416.66	555.55	625	357.14	270.27	434.78	370.37
	K_L	0.24	0.15	0.12	179.77	0.04	0.12	5813.95	207.90
	R^2	0.989	0.983	0.947	0.994	0.998	0.983	0.999	0.996
Freundlich isotherm	K_F	3.83	5	4.62	13.02	7.81	7.09	13.24	8.39
	$1/n$	0.55	0.44	0.53	0.09	0.24	0.22	0.02	0.21
	n	1.79	2.27	1.87	10.05	4.02	4.54	37.03	4.56
	R^2	0.909	0.963	0.942	0.926	0.756	0.515	0.757	0.811

Adsorption isotherm studies are crucial for evaluating the effectiveness of the adsorption process. The amount of adsorption uptake is predicted using the isotherms, according to Wang et al. [22], and the most common models, Langmuir and Freundlich, were used in this study. The parameters related to the studied isotherms are shown in Table 2. The best fit for the experimental data is the Langmuir isotherm, as shown by the highest determination coefficients R^2, achieved for both dyes, which indicates a monolayer adsorption process occurring on a homogenous surface [14].

Additionally, from the values in Table 2, it is shown that the CR dye is more adsorbed than the DR dye onto the adsorbent surface for all the studied films. These results indicate a better affinity of the CR dye molecules with the Alg/Cs biofilms.

To confirm the adsorption potential of the prepared films towards CR and DR dyes, a comparative analysis of their maximum adsorption capacity (specifically for M4 and M5) was conducted, and the results have been documented in Table 3 alongside various similar adsorbents reported in the existing literature. From the data presented in Table 3, it is evident that the composite films Alg/Cs exhibit noteworthy adsorption performance.

Table 3. Adsorption capacities of CR and DR dyes on various adsorbents.

	Adsorption Capacity (mg g^{-1})		
	CR	**DR**	**Ref.**
PVA/SA/ZSM-5 zeolite membrane	5.33	NA	[41]
Lignin/chitosan beads	173	NA	[42]
Calcium alginate beads/nano-geothite	181.1	NA	[43]
Nano-ZnO/chitosan	120	NA	[44]
Titanium dioxide nanoparticles(TiO_2NPs)	NA	92.17% *	[19]
Sodium alginate and polypyrrole composites with algal dead biomass	77.27	NA	[45]
Novel cyanognanidine-modified chitosan CCs	666.67	NA	[46]
Chitosane and laponite based nanocomposites	390.3	NA	[47]
Alg/Cs film M4	555.55	434.78	This work
Alg/Cs film M5	625	370.37	This work

Note(s): * removal efficiency.

3.3.6. Effect of Temperature and Thermodynamic Study

Temperature is a crucial factor that impacts the adsorption capacity, as noted in the literature [4]. Therefore, the effect of temperature on the adsorption capacities of Alg/Cs biofilms towards CR and DR dyes was investigated within a range of 285 K to 305 K, and the outcomes are illustrated in Figure 8c. Generally, the maximum adsorption capacity for both CR and DR dyes was observed at room temperature (293 K) for most adsorbed films. Conversely, for M4 and M5 films, the adsorption of CR and DR increased as the temperature rose, until it reached 313 K, indicating that the adsorption process was favorable at high temperatures. Similar findings were observed by Shi et al. [48], who reported a maximum removal efficiency of approximately 95% at a high temperature of 308 K when studying the adsorption capacity of Direct Blue15 by porous Cs/Ha films.

The thermodynamic parameters, such as standard free energy change (ΔG°), change in enthalpy (ΔH°) and entropy change (ΔS°), were determined by using equations given in Table 1. ΔH° and ΔS° can be calculated from the slope and intercept of the linear plot $\ln(K^{o})$ versus 1/T, respectively. The results are displayed in Table 4. The negative values of ΔG° obtained for all Alg/Cs films highlight the spontaneity and feasibility of the adsorption process, while the negative values of enthalpy change ΔH°, suggesting the exothermic nature of the process. Additionally, the positive values of ΔS° indicate an increase in randomness on the interface (solid–liquid). These favorable results signify an effective adsorption process utilizing the synthesized Alg/Cs films.

Table 4. Thermodynamic parameters.

		CR			DR		
	T (K)	**ΔS° ($J \cdot mol^{-1} \cdot k^{-1}$)**	**ΔH° ($kJ \cdot mol^{-1}$)**	**ΔG° ($kJ \cdot mol^{-1}$)**	**ΔS° ($J \cdot mol^{-1} \cdot k^{-1}$)**	**ΔH° ($kJ \cdot mol^{-1}$)**	**ΔG° ($kJ \cdot mol^{-1}$)**
M2	283	0.07	2.66	−18.24	0.14	−24.56	−66.21
	293			−18.98			−67.68
	313			−20.46			−70.62
M3	283	0.12	−15.82	−51.19	0.19	−38.82	−94.68
	293			−52.44			−96.66
	313			−54.94			−100.61
M4	283	0.05	2.871	−13.41	0.19	−38.55	−93.92
	293			−13.99			−95.87
	313			−15.14			−99.79
M5	283	0.16	−29.04	−75.69	0.18	−35.74	−87.78
	293			−77.33			−89.62
	313			−80.63			−93.29

3.4. Adsorption Mechanism

To further elucidate the adsorption mechanism, the FTIR spectra of Alg/Cs films after CR and DR adsorption were performed (Figure S2). The characteristic bands of CR and DR dyes appeared on the spectra of Alg/Cs films after adsorption, confirming that both dyes were successfully adsorbed by the films. The asymmetry stretching vibration of S-O of (SO_3^-) group at around 1370 and 1150 cm^{-1} and the peak of aromatic C=C was observed around 1580 cm^{-1} for both CR- and DR-associated specters after adsorption.

Furthermore, it was observed that certain characteristic peaks underwent shifts, and their intensity was reduced, which can be attributed to either electrostatic interactions between the film surface and dyes or hydrogen bonding [3]. For instance, the stretching bands of OH and NH_2 groups were shifted from 3246–3284 cm^{-1} (before adsorption) to 3365–3300 cm^{-1} (after adsorption), affirming the hydrogen bonding among the films and

dye molecules. The surface of the film loaded with CR dye (Figure 9a) is significantly different from that before adsorption, where we can clearly see the presence of irregular particles attached to the film surface, evidence of dye particle deposition.

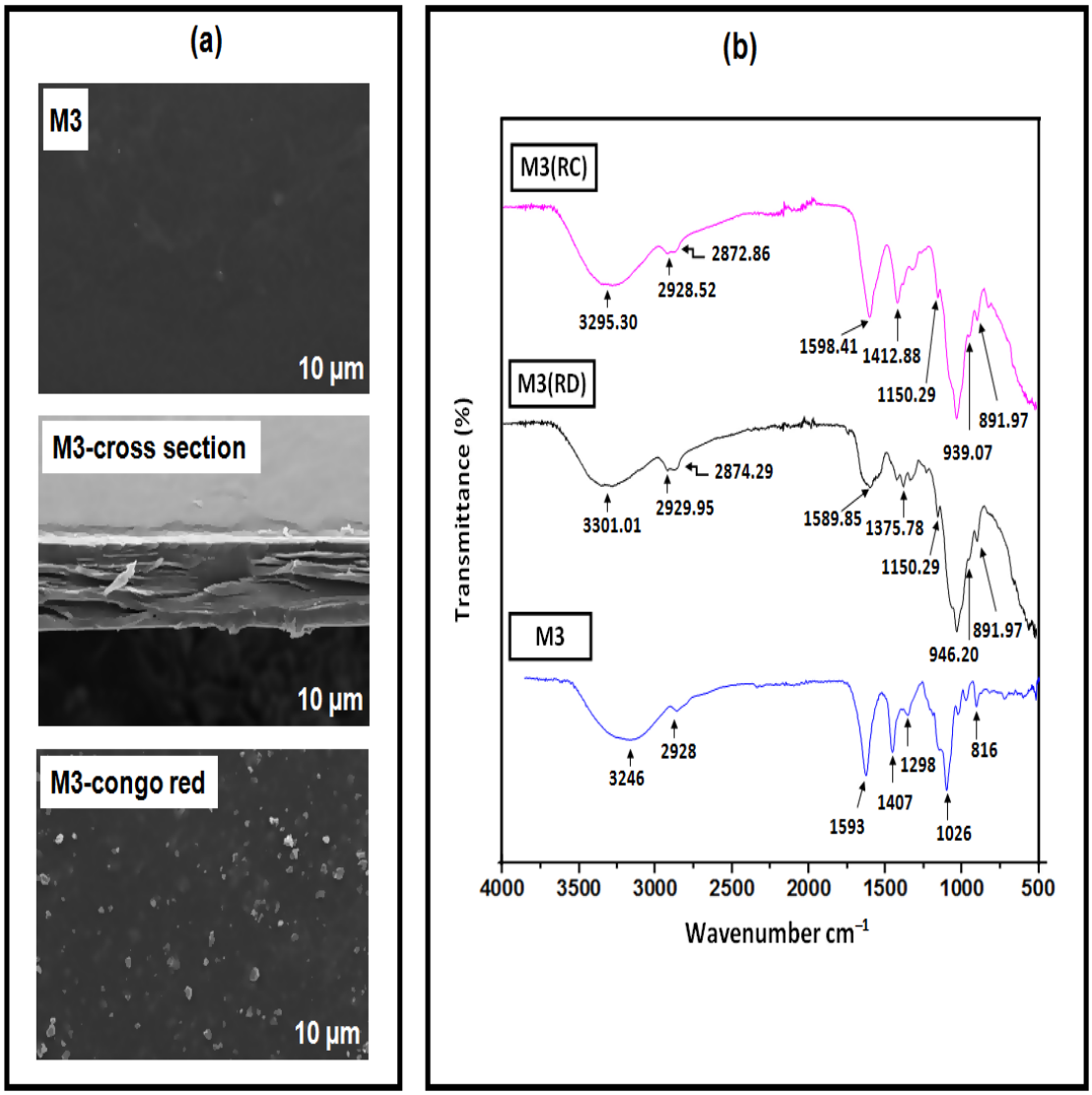

Figure 9. SEM image (**a**) and FTIR spectra (**b**) of M3 before and after dye adsorption.

Based on the obtained results, we can conclude that the adsorption mechanism is mainly controlled by electrostatic interactions and hydrogen bonds between the film surface and dyes. Figure 10 represents an illustrative scheme for the possible adsorption mechanism.

3.5. Correlation between the Swelling Behavior and Adsorption Process at Different pH

The relationship between the amount of adsorbed CR and DR dyes and the swelling characteristics of M4 film is shown in Figure 11. It can be seen from the graph that the swelling capacity increased by the increasing of adsorption. These findings demonstrate the exceptional water retention ability of Alg/Cs films, which may potentially be a sign of superior adsorption abilities. Additionally, the pH can play a significant role in determining the adsorption behavior of dyes. Saradyen et al. [49] have also reported similar correlations between swelling behavior and adsorption properties of poly(hydroxamic acid) hydrogels towards organic dyes. Additionally, Hu et al. [50] found that increasing the swelling capacity promotes the films' surface area to increase, which fully exposes the adsorption

sites to CR dyes. As a result, the films' high capacity for swelling enhanced the dyes' adsorption capacity.

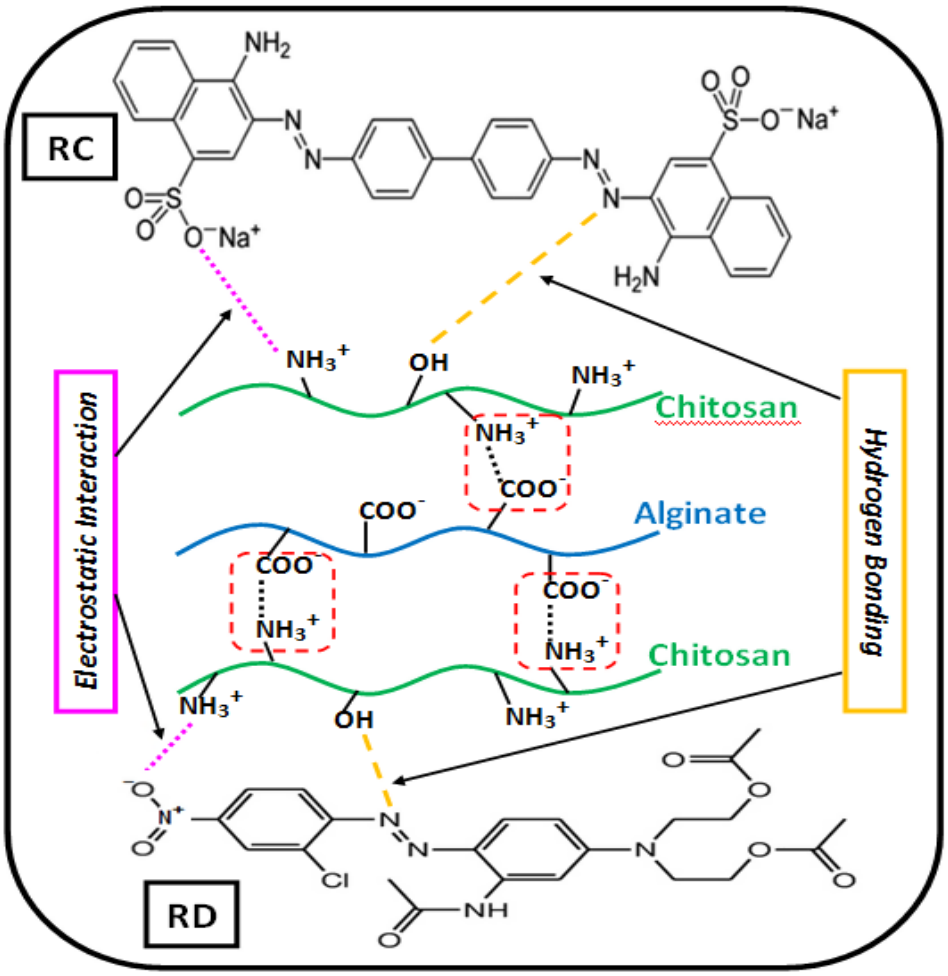

Figure 10. A possible mechanism for the adsorption of CR and DR dyes onto the Alg/Cs film.

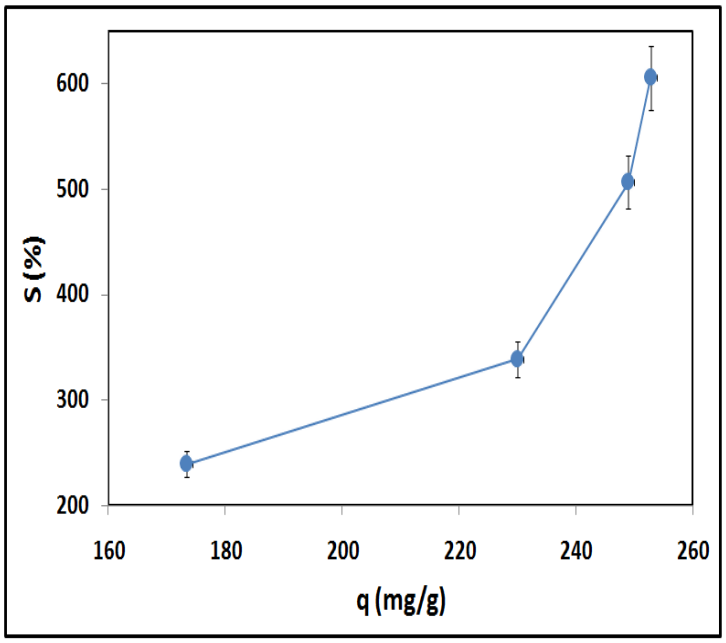

Figure 11. Correlation between swelling behavior and adsorption capacity of M4.

4. Conclusions

Adsorbent films prepared by facile association between two natural and abundant polysaccharides, namely, alginate and chitosan, were successfully manufactured, providing high efficiency to remove Congo red and Coralene Dark Red2B, two toxic azo-dyes highly present in textile wastewaters. The adsorption potential was shown to be closely related to the mass ratio of Cs to Alg, and increasing ratio of Cs can significantly improve the adsorption capacity of composite film. Thus, the two films, M4 (Alg/Cs ratio: 25/75) and M5 (0/100), revealed high adsorption capacities of 842.36 and 315.52 mg/g for CR and DR, respectively, in a short time of 45–50 min, indicating that these composite films could be good candidates for dye removal on a commercial scale. Acidic medium (pH = 4), room temperature and film thickness of 0.45–0.49 mm were found to be suitable conditions for the removal of a maximum initial dye concentration of 300 mg/L. The equilibrium experimental data fitted well with the Langmuir isotherm model for both dyes, suggesting a monolayer adsorption on homogeneous surface of Alg/Cs films. In addition, the pseudo-second-order kinetic model was more appropriate to describe CR and DR adsorption onto the composite films, with coefficients of determination near to unity. Results from the thermodynamic analysis highlighted the spontaneity and the exothermic nature of the adsorption process. In view of the obtained results, Alg/Cs films could be regarded as potential bioadsorbents to treat dye-contaminated waters. They could be used as amphoteric adsorbents for the removal of not only anionic dyes, but also for cationic dye removal. Investigations on the regeneration and reuse of these films are currently being undertaken to promote a sustainable treatment of dye-polluted waters.

Supplementary Materials: The following supporting information can be downloaded at: https://www.mdpi.com/article/10.3390/w15091709/s1, Table S1: Zeta potential of Alg/Cs films at different pH; Figure S1: Point of zero charge pH_{pzc} of Alg/Cs films; Figure S2: FTIR spectra of Alg/Cs films after adsorption (a) RC dye (b) RD dye.

Author Contributions: Conceptualization, A.M., S.B. and Z.B.; Methodology, S.B., Z.B. and N.B.; Validation, A.M., S.B. and A.A.B.; Formal Analysis, A.M., S.B., S.D.T. and Ö.T.; Investigation, A.M. and S.B.; Data Curation, H.M. and Z.B.; Writing—Original Draft Preparation, A.M. and S.B.; Writing—Review and Editing, H.M., S.D.T. and Z.B. All authors have read and agreed to the published version of the manuscript.

Funding: This research received no external funding.

Data Availability Statement: Data available on request.

Acknowledgments: The authors would like to thank the Directorate General of Scientific Research and Technological Development (DGRSDT) and the Ministry of Higher Education and Scientific Research (MESRS), Algeria, for scientific support.

Conflicts of Interest: The authors declare no conflict of interest.

References

1. Mia, R.; Selim, M.D.; Shamim, A.M.; Chowdhury, M.; Sultana, S.; Armin, M.; Hossain, M.; Akter, R.; Dey, S.; Naznin, H. Review on various types of pollution problem in textile dyeing & printing industries of Bangladesh and recommandation for mitigation. *J. Text. Eng. Fash. Technol.* **2019**, *5*, 62–65. [CrossRef]
2. Zhou, Y.; Lu, J.; Zhou, Y.; Liu, Y. Recent advances for dyes removal using novel adsorbents: A review. *Environ. Pollut.* **2019**, *252*, 352–365. [CrossRef] [PubMed]
3. Samsami, S.; Mohamadizaniani, M.; Sarrafzadeh, M.-H.; Rene, E.R.; Firoozbahr, M. Recent advances in the treatment of dye-containing wastewater from textile industries: Overview and perspectives. *Process. Saf. Environ. Prot.* **2020**, *143*, 138–163. [CrossRef]
4. Lellis, B.; Fávaro-Polonio, C.Z.; Pamphile, J.A.; Polonio, J.C. Effects of textile dyes on health and the environment and bioremediation potential of living organisms. *Biotechnol. Res. Innov.* **2019**, *3*, 275–290. [CrossRef]
5. Al-Tohamy, R.; Ali, S.S.; Li, F.; Okasha, K.M.; Mahmoud, Y.A.-G.; Elsamahy, T.; Jiao, H.; Fu, Y.; Sun, J. A critical review on the treatment of dye-containing wastewater: Ecotoxicological and health concerns of textile dyes and possible remediation approaches for environmental safety. *Ecotoxicol. Environ. Saf.* **2022**, *231*, 113160. [CrossRef]

6. Bharathi, K.S.; Ramesh, S.T. Removal of dyes using agricultural waste as low-cost adsorbents: A review. *Appl. Water Sci.* **2013**, *3*, 773–790. [CrossRef]
7. Deng, L.; Shi, Z.; Peng, X.; Zhou, S. Magnetic calcinated cobalt ferrite/magnesium aluminum hydrotalcite composite for enhanced adsorption of methyl orange. *J. Alloys Compd.* **2016**, *688*, 101–112. [CrossRef]
8. Nazir, M.A.; Najam, T.; Zarin, K.; Shahzad, K.; Javed, M.S.; Jamshaid, M.; Bashir, M.A.; Shah, S.S.A.; Rehman, A.U. Enhanced adsorption removal of methyl orange from water by porous bimetallic Ni/Co MOF composite: A systematic study of adsorption kinetics. *Int. J. Environ. Anal. Chem.* **2021**, 1–16. [CrossRef]
9. Nazir, M.A.; Najam, T.; Shahzad, K.; Wattoo, M.A.; Hussain, T.; Tufail, M.K.; Shah, S.S.A.; Rehman, A.U. Heterointerface engineering of water stable ZIF-8@ ZIF-67: Adsorption of rhodamine B from water. *Surf. Interfaces* **2022**, *34*, 102324. [CrossRef]
10. Haounati, R.; Alakhras, F.; Ouachtak, H.; Saleh, T.A.; Al-Mazaideh, G.; Alhajri, E.; Jada, A.; Hafid, N.; Addi, A.A. Synthesized of Zeolite@Ag_2O Nanocomposite as Superb Stability Photocatalysis Toward Hazardous Rhodamine B Dye from Water. *Arab. J. Sci. Eng.* **2023**, *48*, 169–179. [CrossRef]
11. Ouachtak, H.; El Guerdaoui, A.; El Haouti, R.; Haounati, R.; Ighnih, H.; Toubi, Y.; Alakhras, F.; Rehman, R.; Hafid, N.; Addi, A.A.; et al. Combined molecular dynamics simulations and experimental studies of the removal of cationic dyes on the eco-friendly adsorbent of activated carbon decorated montmorillonite Mt@AC. *RSC Adv.* **2023**, *13*, 5027–5044. [CrossRef] [PubMed]
12. Dutta, S.; Gupta, B.; Srivastava, S.K.; Gupta, A.K. Recent advances on the removal of dyes from wastewater using various adsorbents: A critical review. *Mater. Adv.* **2021**, *2*, 4497–4531. [CrossRef]
13. Karthikeyan, P.; Banu, H.A.T.; Meenakshi, S. Synthesis and characterization of metal loaded chitosan-alginate biopolymeric hybrid beads for the efficient removal of phosphate and nitrate ions from aqueous solution. *Int. J. Biol. Macromol.* **2019**, *130*, 407–418. [CrossRef]
14. de Moraes, M.A.; Cocenza, D.S.; Vasconcellos, F.D.C.; Fraceto, L.; Beppu, M.M. Chitosan and alginate biopolymer membranes for remediation of contaminated water with herbicides. *J. Environ. Manag.* **2013**, *131*, 222–227. [CrossRef]
15. Javadian, H.; Ruiz, M.; Saleh, T.A.; Sastre, A.M. Ca-alginate/carboxymethyl chitosan/$Ni_0.2Zn_0.2Fe_2.6O_4$ magnetic bionanocomposite: Synthesis, characterization and application for single adsorption of Nd^{+3}, Tb^{+3}, and Dy^{+3} rare earth elements from aqueous media. *J. Mol. Liq.* **2020**, *306*, 112760. [CrossRef]
16. da Costa, T.B.; da Silva, M.G.C.; Vieira, M.G.A. Crosslinked alginate/sericin particles for bioadsorption of ytterbium: Equilibrium, thermodynamic and regeneration studies. *Int. J. Biol. Macromol.* **2020**, *165*, 1911–1923. [CrossRef]
17. Bhuvaneshwari, S.; Sruthi, D.; Sivasubramanian, V. Development and characterization of chitosan film. *Int. J. Eng. Res. Appl.* **2011**, *1*, 8.
18. Zhao, X.; Wang, X.; Lou, T. Preparation of fibrous chitosan/sodium alginate composite foams for the adsorption of cationic and anionic dyes. *J. Hazard. Mater.* **2020**, *403*, 124054. [CrossRef]
19. Singh, A.; Goyal, V.; Singh, J.; Rawat, M. Structural, morphological, optical and photocatalytic properties of green synthesized TiO_2 NPs. *Curr. Res. Green Sustain. Chem.* **2020**, *3*, 100033. [CrossRef]
20. Córdoba, L.J.P.; Sobral, P.J. Physical and antioxidant properties of films based on gelatin, gelatin-chitosan or gelatin-sodium caseinate blends loaded with nanoemulsified active compounds. *J. Food Eng.* **2017**, *213*, 47–53. [CrossRef]
21. Nordine, N.; El Bahri, Z.; Sehil, H.; Fertout, R.I.; Rais, Z.; Bengharez, Z. Lead removal kinetics from synthetic effluents using Algerian pine, beech and fir sawdust's: Optimization and adsorption mechanism. *Appl. Water Sci.* **2016**, *6*, 349–358. [CrossRef]
22. Wang, J.; Guo, X. Adsorption kinetic models: Physical meanings, applications, and solving methods. *J. Hazard. Mater.* **2020**, *390*, 122156. [CrossRef]
23. Li, K.; Zhu, J.; Guan, G.; Wu, H. Preparation of chitosan-sodium alginate films through layer-by-layer assembly and ferulic acid crosslinking: Film properties, characterization, and formation mechanism. *Int. J. Biol. Macromol.* **2019**, *122*, 485–492. [CrossRef]
24. Boudouaia, N.; Bengharez, Z.; Jellali, S. Preparation and characterization of chitosan extracted from shrimp shells waste and chitosan film: Application for Eriochrome black T removal from aqueous solutions. *Appl. Water Sci.* **2019**, *9*, 91. [CrossRef]
25. Gazori, T.; Khoshayand, M.R.; Azizi, E.; Yazdizade, P.; Nomani, A.; Haririan, I. Evaluation of Alginate/Chitosan nanoparticles as antisense delivery vector: Formulation, optimization and in vitro characterization. *Carbohydr. Polym.* **2009**, *77*, 599–606. [CrossRef]
26. Hoang, T.; Ramadass, K.; Loc, T.T.; Mai, T.T.; Giang, L.D.; Thang, V.V.; Tuan, T.M.; Chinh, N.T. Novel Drug Delivery System Based on Ginsenoside Rb1 Loaded to Chitosan/Alginate Nanocomposite Films. *J. Nanosci. Nanotechnol.* **2019**, *19*, 3293–3300. [CrossRef]
27. Elanchezhiyan, S.S.D.; Sivasurian, N.; Meenakshi, S. Efficacy of La3+entrapped chito- san bio-polymeric matrix for the recovery of oil from oil-in-water emulsion. *J. Appl. Polym. Sci.* **2016**, *133*, 43218–43231. [CrossRef]
28. Bibi, A.; Rehman, S.-U.; Faiz, R.; Akhtar, T.; Nawaz, M.; Bibi, S. Effect of surfactants on swelling capacity and kinetics of alginate-chitosan/CNTs hydrogel. *Mater. Res. Express* **2019**, *6*, 085065. [CrossRef]
29. Li, C.; Xu, L.; Zhai, M.; Peng, J.; Li, J. Overshooting effect of poly(dimethylaminoethyl methacrylate) hydrogels. *J. Appl. Polym. Sci.* **2011**, *120*, 2027–2033. [CrossRef]
30. Yin, Y.; Ji, X.; Dong, H.; Ying, Y.; Zheng, H. Study of the swelling dynamics with overshooting effect of hydrogels based on sodium alginate-g-acrylic acid. *Carbohydr. Polym.* **2008**, *71*, 682–689. [CrossRef]
31. Alsamman, M.T.; Sánchez, J. Chitosan- and Alginate-Based Hydrogels for the Adsorption of Anionic and Cationic Dyes from Water. *Polymers* **2022**, *14*, 1498. [CrossRef]
32. Chen, T.; Liu, H.; Gao, J.; Hu, G.; Zhao, Y.; Tang, X.; Han, X. Efficient Removal of Methylene Blue by Bio-Based Sodium Alginate/Lignin Composite Hydrogel Beads. *Polymers* **2022**, *14*, 2917. [CrossRef] [PubMed]

33. Ahmed, I.A.; Ragab, A.H.; Habila, M.A.; Alomar, T.S.; Aljuhani, E.H. Equilibrium and Kinetic Study of Anionic and Cationic Pollutants Remediation by Limestone–Chitosan–Alginate Nanocomposite from Aqueous Solution. *Molecules* **2021**, *26*, 2586. [CrossRef] [PubMed]
34. Bhatti, H.N.; Mahmood, Z.; Kausar, A.; Yakout, S.M.; Shair, O.H.; Iqbal, M. Biocomposites of polypyrrole, polyaniline and sodium alginate with cellulosic biomass: Adsorption-desorption, kinetics and thermodynamic studies for the removal of 2,4-dichlorophenol. *Int. J. Biol. Macromol.* **2020**, *153*, 146–157. [CrossRef]
35. Omraei, M.; Esfandian, H.; Katal, R.; Ghorbani, M. Study of the removal of Zn(II) from aqueous solution using polypyrrole nanocomposite. *Desalination* **2011**, *271*, 248–256. [CrossRef]
36. Ahmed, M.; Khafagy, R.M.; Bishay, S.T.; Saleh, N. Effective dye removal and water purification using the electric and magnetic $Zn_0.5Co_0.5A_{l0}.5Fe_1.46La0.04O_4$/polymer core–shell nanocomposites. *J. Alloys Compd.* **2013**, *578*, 121–131. [CrossRef]
37. Saikia, M.D.; Dutta, N. Adsorption affinity of certain biomolecules onto polymeric resins: Effect of solute chemical nature. *React. Funct. Polym.* **2008**, *68*, 33–38. [CrossRef]
38. Korzhikov-Vlakh, V.; Krylova, M.; Sinitsyna, E.; Ivankova, E.; Averianov, I.; Tennikova, T.B. Hydrogel Layers on the Surface of Polyester-Based Materials for Improvement of Their Biointeractions and Controlled Release of Proteins. *Polymers* **2016**, *8*, 418. [CrossRef]
39. Shaban, M.; Abukhadra, M.R.; Khan, A.A.P.; Jibali, B.M. Removal of Congo red, methylene blue and Cr(VI) ions from water using natural serpentine. *J. Taiwan Inst. Chem. Eng.* **2018**, *82*, 102–116. [CrossRef]
40. Kataria, N.; Garg, V. Removal of Congo red and Brilliant green dyes from aqueous solution using flower shaped ZnO nanoparticles. *J. Environ. Chem. Eng.* **2017**, *5*, 5420–5428. [CrossRef]
41. Radoor, S.; Karayil, J.; Parameswaranpillai, J.; Siengchin, S. Removal of anionic dye Congo red from aqueous environment using polyvinyl alcohol/sodium alginate/ZSM-5 zeolite membrane. *Sci. Rep.* **2020**, *10*, 15452. [CrossRef] [PubMed]
42. Han, X.; Li, R.; Miao, P.; Gao, J.; Hu, G.; Zhao, Y.; Chen, T. Design, Synthesis and Adsorption Evaluation of Bio-Based Lignin/Chitosan Beads for Congo Red Removal. *Materials* **2022**, *15*, 2310. [CrossRef] [PubMed]
43. Munagapati, V.S.; Kim, D.-S. Equilibrium isotherms, kinetics, and thermodynamics studies for congo red adsorption using calcium alginate beads impregnated with nano-goethite. *Ecotoxicol. Environ. Saf.* **2017**, *141*, 226–234. [CrossRef] [PubMed]
44. Jiang, R.; Zhu, H.-Y.; Fu, Y.-Q.; Jiang, S.-T.; Zong, E.-M.; Zhu, J.-Q.; Zhu, Y.-Y.; Chen, L.-F. Colloidal CdS sensitized nano-ZnO/chitosan hydrogel with fast and efficient photocatalytic removal of congo red under solar light irradiation. *Int. J. Biol. Macromol.* **2021**, *174*, 52–60. [CrossRef] [PubMed]
45. Maqbool, M.; Sadaf, S.; Bhatti, H.N.; Rehmat, S.; Kausar, A.; Alissa, S.A.; Iqbal, M. Sodium alginate and polypyrrole composites with algal dead biomass for the adsorption of Congo red dye: Kinetics, thermodynamics and desorption studies. *Surf. Interfaces* **2021**, *25*, 101183. [CrossRef]
46. Al-Harby, N.F.; Albahly, E.F.; Mohamed, N.A. Kinetics, Isotherm and Thermodynamic Studies for Efficient Adsorption of Congo Red Dye from Aqueous Solution onto Novel Cyanoguanidine-Modified Chitosan Adsorbent. *Polymers* **2021**, *13*, 4446. [CrossRef]
47. Xu, G.; Zhu, Y.; Wang, X.; Wang, S.; Cheng, T.; Ping, R.; Cao, J.; Lv, K. Novel chitosan and Laponite based nanocomposite for fast removal of Cd(II), methylene blue and Congo red from aqueous solution. *E Polym.* **2019**, *19*, 244–256. [CrossRef]
48. Shi, C.; Lv, C.; Wu, L.; Hou, X. Porous chitosan/hydroxyapatite composite membrane for dyes static and dynamic removal from aqueous solution. *J. Hazard. Mater.* **2017**, *338*, 241–249. [CrossRef]
49. Saraydın, D.; Işıkver, Y.; Karadağ, E. A Study on the Correlation Between Adsorption and Swelling for Poly(Hydroxamic Acid) Hydrogels-Triarylmethane Dyes Systems. *J. Polym. Environ.* **2018**, *26*, 3924–3936. [CrossRef]
50. Hu, X.-S.; Liang, R.; Sun, G. Super-adsorbent hydrogel for removal of methylene blue dye from aqueous solution. *J. Mater. Chem. A* **2018**, *6*, 17612–17624. [CrossRef]